Powder Metallurgy and Metal Ceramics, Vol. 48, Nos. 3-4, 2009

MECHANICAL PROPERTIES OF POWDER TITANIUM AT DIFFERENT PRODUCTION STAGES. III. CONTACT FORMATION IN POWDER TITANIUM BASED ON EXAMINATION OF MECHANICAL PROPERTIES IN SINTERING

Yu. N. Podrezov,[1,2] V. A. Nazarenko,[1] A. V. Vdovichenko,[1] V. I. Danilenko,[1] O. S. Koryak,[1] and Ya. I. Evich[1]

UDC 621.762.4:620.18.539.4

The mechanical properties of porous titanium samples in vacuum sintering are analyzed. The effect of porosity and initial powder size on conductivity, static and dynamic elastic moduli, ultimate strength, and strain to failure is examined for sintering temperatures between 300 and 1200°C. The quality of contact in materials in different structural states is subjected to a comparative analysis.

Keywords*: porosity, mechanical properties, powder titanium, resistivity, elastic modulus.*

INTRODUCTION

One of the major processes of producing powder titanium involves pressing of the powder and subsequent sintering of the billet. The compaction and properties of cold-pressed billets are considered in [1, 2]. To make a high-quality powder part, perfect contact should necessarily form during sintering.

The objective of this paper is to examine how the mechanical properties vary during sintering of titanium powder compacts and to analyze how contact formation depends on sintering temperature, porosity, and particle size.

The quality of electrical contact was determined by conductivity, the quality of mechanical contact by relative elastic modulus, and the quality of physical contact by true strain to failure (proportional to fracture toughness). To compare the formation of contacts in compacts in different aggregate states, we used classical notions of contact formation theory (Frenkel [3], Pines [4], Geguzin [5]) further developed by Skorokhod and colleagues [6–8]. According to these notions, interparticle space is filled due to creep under capillary pressure P, which is inversely proportional to the radius of curvature R of the contact area [5]:

$$P = 2\alpha/R, \tag{1}$$

where α is the surface energy.

To compare the formation of contacts in materials with different structures, relationship should be established between the relative size of the contact area and mechanical properties. This is especially important for

[1]Frantsevich Institute for Problems of Materials Science, National Academy of Sciences of Ukraine, Kiev, Ukraine.

[2]To whom correspondence should be addressed; e-mail: podrezov@materials.kiev.ua.

Translated from Poroshkovaya Metallurgiya, Vol. 48, No. 3–4 (466), pp. 98–111, 2009. Original article submitted April 22, 2007.

analyzing pressed compacts whose sintering follows the deformation of particles; as a result, contact boundaries become of complex shape and are stochastically distributed over particles. A scanning microscope cannot be used to measure the size of the contact spot in such materials (including powder titanium), so the measured mechanical properties provide indirect but unique information on the total contact area.

The simplest geometrical models that describe contact formation in powder materials consisting of spherical particles [9, 10] associate conductivity or elastic modulus with contact radius squared. Skorokhod and coauthors [11, 12] analyzed more profoundly the relation between the mechanical properties and size of contact between particles. Based on Holm's theory [13] on the electrical properties of a single contact, linear dependence of conductivity and relative radius of contact at early stages of its formation was determined in [11]. The paper [12] considers how the contact radius influences the relative elastic modulus and shows that the relative elastic modulus in a powder body is also proportional to the contact radius based on the solution of the Hertz problem (compression of two elastic spherical particles in contact).

Existing phenomenological theories and numerous experiments on powder materials with stochastically distributed defects show a close relationship between the size of contact and mechanical properties.

MATERIAL AND PROCEDURE

We used PTÉS titanium powder, which was sieved into –063, –063+05, –05+0315, –0315+02, and –02+01 size fractions. The properties of the starting powders are described in [1]. Compacts as $5 \times 7 \times 45$ mm rectangular bars were produced by double-action pressing in a closed die mold with no stops. Samples with a porosity of 0.05 to 0.4 were produced under different compaction pressures. The compacts were then sintered in an SShVL-01 vacuum furnace at 300, 500, 700, 1000, and 1200°C.

Electric resistance was determined using a standard quadripole (two-port) network and an R4833 measuring device. For mechanical tests, a universal computer-aided Ceram test system, which automatically plotted the stress–strain curve, was used. Samples for the four-point bending test were rectangular bars with the sizes equal to those of the compacts. The distance between the far supports was 40 mm and between the central ones 20 mm. The following mechanical properties in bending were determined: Young's modulus E, limit of proportionality σ_{001}, yield stress σ_{02}, ultimate strength σ_s, and failure strain e_s. The samples sintered at 1000 and 1200ºC were also subjected to uniaxial tension tests. In this case, we determined the yield stress and ultimate strength and calculated the failure strain as follows: $e_s = \ln(S_i/S_f)$, where S_i and S_f are the initial and final cross-sectional areas of the sample, respectively.

In addition, the dynamic Young's modulus (E_{dyn}) of the samples after sintering was calculated from the frequency of the first transverse mode of a sample cantilevered on a VÉDS-200 shaker table and then was corrected using the longitudinal-resonance frequency as described in [14].

EXPERIMENTAL RESULTS

Experiments were performed on no fewer than three samples for each structural state and sintering temperature. The measured resistivity and mechanical properties for each powder fraction were averaged and summarized in tables depending on porosity and sintering temperature. As an example, Table 1 summarizes data for –05+0315 fraction.

The resistivity and mechanical properties vary widely depending on the structural state and sintering temperature (Table 1).

The dependence of electrical and mechanical properties on structural and process parameters permits analyzing the patterns of contact formation. To asses the quality of contacts, we used the method proposed by Skorokhod [6], which he further developed together with Solonin [7]. For this purpose, we compared the properties of a perfectly sintered material and a material sintered in different conditions. With this approach, the quality of electrical contact is characterized by the variation in conductivity and the quality of mechanical contact is determined by the variation in elastic modulus. To define the perfect (physical) contact, the variation in true failure strain is proposed to be examined.

TABLE 1. Properties of –05+0315 Titanium Powder Samples Sintered at Different Temperatures

θ, %	$\rho \cdot 10^8$, Ω · m	E_{dyn}, GPa	E, GPa	σ_{001}, MPa	σ_{02}, MPa	σ_s, MPa	$e_s \cdot 10^2$, %	K_s, %	K_E, %	K_e, %
Green										
5	642.4	14.0	10.30	10.40	21.50	31.90	0.48	0	0	0
10	961.8	10.0	6.10	4.75	16.50	20.40	0.47	0	0	0
20	1272.1	2.7	2.30	1.79	5.95	7.14	0.42	0	0	0
30	2902.0	1.5	0.91	0.61	2.36	2.83	0.38	0	0	0
40	8175.3	–	0.24	0.16	0.36	0.47	0.25	0	0	0
Sintering temperature 300°C										
5	493.8	14.1	10.3	10.50	21.70	32.00	0.45	2.4	0	0
10	687.1	9.8	6.5	4.80	16.40	20.50	0.42	2.3	0	0
20	960.0	2.8	2.2	1.90	6.00	7.20	0.41	1.6	0	0
30	2252.1	1.4	0.8	0.60	2.50	2.90	0.39	0.8	0	0
40	5450.1	–	0.3	0.18	0.35	0.45	0.28	0.6	0	0
Sintering temperature 500°C										
5	143.1	24.70	11.30	16.00	33.0	38.0	0.44	28.5	1.1	0
10	244.1	11.06	6.40	9.00	20.7	23.7	0.41	17.0	0.4	0
20	446.7	3.40	2.60	3.60	8.7	8.9	0.23	9.6	0	0
30	864.7	1.27	0.50	0.60	–	1.4	0.13	6.4	0	0
40	2900.1	0.22	0.15	0.25	–	0.4	0.07	2.2	0	0
Sintering temperature 700°C										
5	62.50	34.01	42.000	46.00	115.10	121.30	0.41	75.9	35.6	0
10	88.81	30.50	36.000	32.50	79.50	94.00	0.46	57.0	28.7	0
20	164.83	17.00	7.240	9.20	20.68	22.12	0.31	34.9	7.3	0
30	328.26	5.50	2.100	3.65	6.65	7.40	0.21	21.3	2.2	0
40	850.00	0.60	0.255	0.53	1.00	2.90	0.20	10.3	0	0
Sintering temperature 1000°C										
5	47.30	90.5	93.5	195.5	300.1	330.2	108.00	100.0	93.5	32.7
10	54.30	66.5	82.5	147.0	262.5	390.0	4.00	96.9	92.0	28.2
20	69.46	45.0	55.1	73.0	132.0	203.0	2.20	90.3	77.5	26.0
30	93.01	31.5	34.8	48.0	90.1	132.1	0.55	82.1	64.0	18.5
40	158.30	16.3	15.1	17.0	37.1	48.0	0.27	60.7	37.8	6.4
Sintering temperature 1200°C										
5	47.5	99.3	98.9	201.0	310.0	350.1	32.14	100	100	100
10	53.1	85.6	88.0	142.5	260.0	304.0	12.20	100	100	100
20	63.0	53.8	70.0	83.5	147.5	235.0	6.80	100	100	100
30	77.5	34.6	53.5	62.0	113.5	179.0	2.40	100	100	100
40	97.0	19.8	39.5	32.5	61.0	86.0	1.00	100	100	100

To assess the quality of electrical contact, the following formula is used in [6, 7]:

$$\xi_\lambda = \lambda_{ms} / \lambda_{th}, \tag{2}$$

where

$$\lambda_{th} = \lambda_0 (1 - \theta)^{3/2}. \tag{3}$$

Here λ_0 is the conductivity of compact material, θ is porosity.

By analogy, the following relation is used for mechanical contact:

$$\xi_E = E_{ms} / E_{th}, \tag{4}$$

where, according to [15],

$$E_{th} = E_0(1 - \theta)^2. \quad (5)$$

Here E_0 is the elastic modulus of compact material.

By comparing the properties measured at a certain stage of the process with those of the green compact, we may analyze the improvement of contact. The coefficient χ that shows how the contact improves as compared with green compacts may be determined as follows:

$$\chi_\lambda = \lambda_{gr} / \lambda_{ms} \quad (6)$$

for the conductivity and

$$\chi_E = E_{gr} / E_{ms} \quad (7)$$

for the elastic modulus.

It is obvious that the coefficients determined from Eqs. (2), (4), (6), and (7) characterize the evolution of contact from green to ideally sintered state. However, it is difficult to use them to analyze how samples in different structural states are sintered because the conductivity and elastic modulus for distinct structural parameters of compacts vary over substantially different ranges.

Hence, we propose to introduce a relative coefficient to measure the quality of contact to show its percent changes for a comparative analysis. For conductivity, it may be expressed as

$$K_\lambda = [(\lambda_{ms} - \lambda_{gr}) / (\lambda_{th} - \lambda_{gr})] \cdot 100\%. \quad (8)$$

For mechanical contact, the expression becomes

$$K_E = [(E_{ms} - E_{gr}) / (E_{th} - E_{gr})] \cdot 100\%. \quad (9)$$

The value of λ_{th} for titanium samples with different porosities is determined from Eq. (3) taking into account $\lambda_0 = 1/\rho_0$, where $\rho_0 = 45 \cdot 10^{-8}\ \Omega \cdot$ m. The conductivity λ_{gr} of a green compact and the conductivity λ_{ms} of that after sintering at preset temperature are found experimentally.

The coefficient to characterize the properties of mechanical contact may be calculated in the same way. The elastic modulus of a porous body with perfect contact is calculated using Eq. (5) taking into account the elastic modulus of compact titanium $E_0 = 114$ GPa. To study how mechanical and electrical contacts form in materials in different structural states, we compared the temperature dependences of K_E and K_λ.

The formation of physical contact should be studied in the same manner. However, a parameter that would adequately characterize the quality of physical contact needs to be defined first. As shown in [16, 17], perfect mechanical contact by no means always implies good physical contact since, at the instant the mechanical contact forms, there is a region rich of admixtures at the interface of powder particles where a crack may propagate with very low expenditure of energy. Poor contact highly reduces impact strength and fracture toughness as compared with compact materials produced using other processes.

Fracture toughness at –196°C, when fracture occurs by quasi-spalling mechanism, was proposed as a parameter that adequately characterized the quality of physical contact in [16] in studying powder iron. The failure of titanium is peculiar in that it occurs without spalling at any testing temperature, which makes it very difficult to test the fracture toughness of sintered samples. According to the theory of elastic failure, fracture toughness K_{Ic} is associated with other mechanical characteristics as follows [18]:

$$K_{Ic} = n \cdot (\sigma_{02}{}^{3/2} \cdot E \cdot e_s \cdot d)^{1/2}, \quad (10)$$

where n is the strain hardening coefficient, σ_{02} is the yield stress, E is the elastic modulus, e_s is the failure strain, and d is the solid-phase grain size.

Experiments show that although the elastic modulus and yield stress may vary severalfold depending on structural parameters, the true failure strain e_s is a more structure-sensitive characteristic and may change ten- and even hundredfold depending on the quality of contact. Thus, e_s is proposed to characterize the quality of physical contact.

By analogy, imperfect physical contact may be characterized by

$$\xi = e_s^{ms} / e_s^{th}. \quad (11)$$

TABLE 2. Dependence of Strain to Failure on Porosity

e_s	θ				
	0.05	0.10	0.20	0.30	0.40
$e_s^{th}(\theta)$	0.42	0.16	0.076	1.3	0.0057
$e_s^{th}(\theta + f)$	0.32	0.13	0.072	1.3	0.0056

The study [17] on the failure of powder materials shows that the effect of porosity on e_s^{th} may be taken into account using Gurland's equation [19] for dimple fracture:

$$e_s = 1/2 \ln\left\{1 + \frac{k_2^2}{k_1^2}\left[\frac{2}{3}\frac{1+2\theta}{\theta}\exp\left(-\frac{e_s}{2}\right) - 2\right]^2\right\}. \quad (12)$$

If we assume that $k_1 = 1.1$ and $k_2 = 0.012$ for both powder titanium and powder iron [17], the dependence of true strain e_s^{th} on porosity may be determined from Eq. (13) (Table 2). Note that, according to the concept of the elastic failure of powder materials [17], dimples are formed by pores and particles of the second phase whose volume fraction $f = 0.02$.

As previously mentioned, the coefficient that characterizes the properties of physical contact at a given sintering temperature is determined as follows:

$$K_e = [(e_s^{ms} - e_s^{gr})/(e_s^{th} - e_s^{gr})] \cdot 100\%. \quad (13)$$

The conditions in which contacts form may be compared using K_λ, K_E, and K_e for different structural states and their dependences on sintering temperature. The curves are S-shaped and always vary from 0 for the compact to 100% for the perfectly sintered material. To compare different compacts, any specific quality of contact should be selected and sintering temperature at which it formed should be determined. It would be most reasonable to select temperature T_{50} at which the contact is 50% formed or T_{10} at which the contact has improved to the extent it can compensate for its remaining imperfection. This is obviously the case when contact is 10% formed (which corresponds to half the logarithmic scale). Figure 1 shows how to determine such temperatures graphically.

The dependences of the quality of contact on sintering temperature for samples with different porosities produced from powders of different fractions are constructed in the same manner. Figure 2a shows how the quality of electrical contact changes in –05+0315 materials with different porosities and Fig. 2b shows how it changes in compacts with 0.1 porosities for different powder fractions.

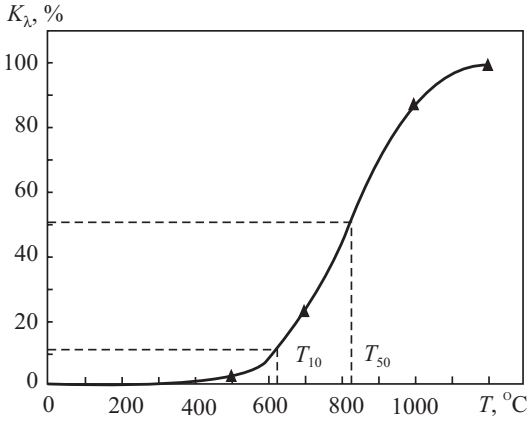

Fig. 1. Dependence of K_λ on sintering temperature of –05+0315 powder samples with 0.1 porosity

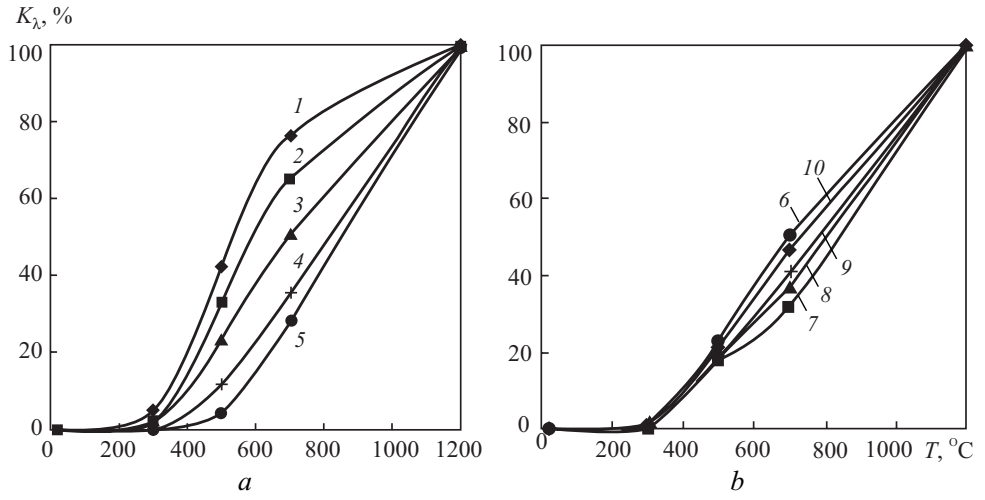

Fig. 2. Dependences of K_λ on sintering temperature: *a*) –05+0315 samples with a porosity of 0.05 (*1*), 0.1 (*2*), 0.2 (*3*), 0.3 (*4*), and 0.4 (*5*); *b*) –063 (*6*), –063+05 (*7*), –05+0315 (*8*), –315+02 (*9*), and –02+01 (*10*) samples with 0.1 porosity

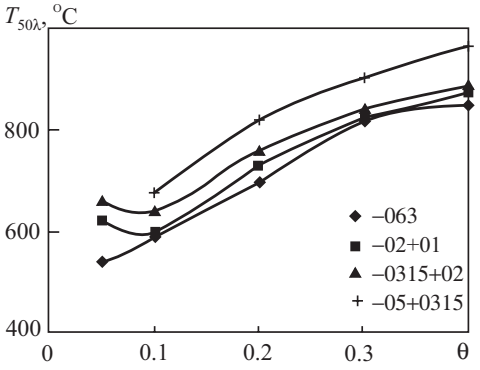

Fig. 3. Dependence of $T_{50\lambda}$ on porosity and particle size

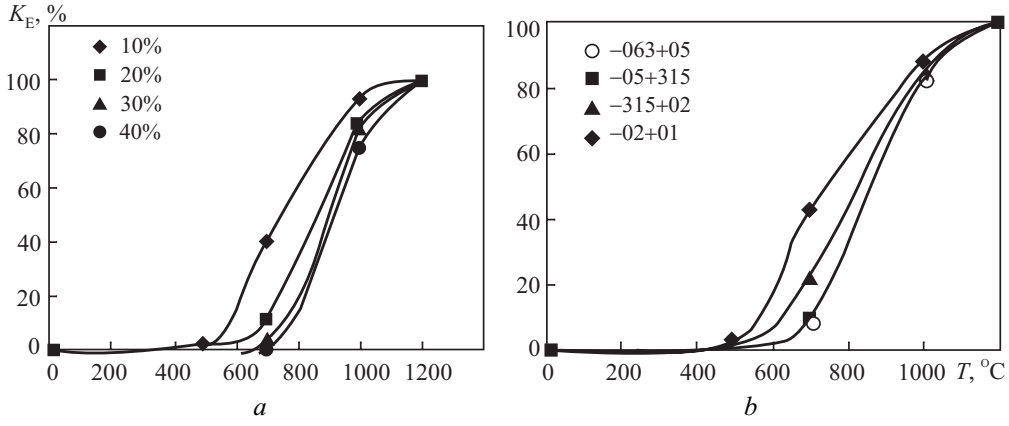

Fig. 4. Dependence of K_E on sintering temperature of –05+0315 samples with different porosities (*a*) and samples of different fractions of titanium powder with 0.1 porosity (*b*)

Temperature $T_{50\lambda}$ was determined for these materials and for compacts with different powder fractions. Its dependence on porosity and particle size is shown in Fig. 3. It is seen that the sinterability of titanium-based material reduces with increasing porosity and particle size.

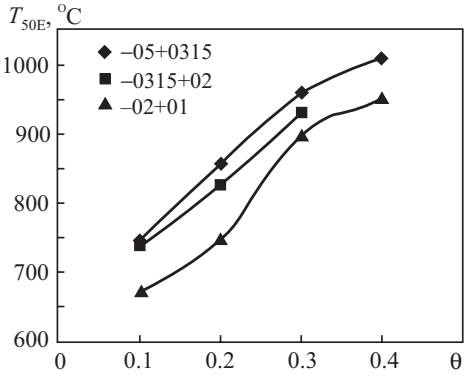

Fig. 5. Dependence of T_{50E} on porosity and particle size

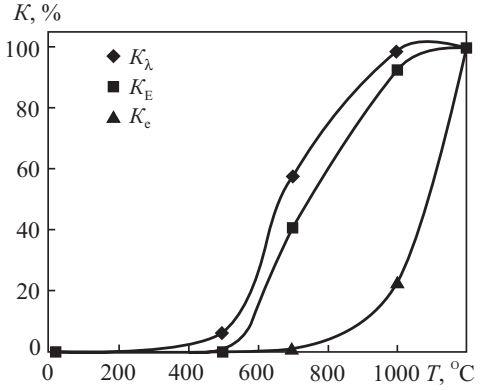

Fig. 6. Dependence of K_λ, K_E, and K_e on sintering temperature of –05+0315 samples with 0.1 porosity

The dependences of the coefficient that characterizes the quality of mechanical contact for titanium compacts with different porosities and particle size are plotted likewise (Fig. 4). The dependences of T_{50E} for all materials in question have also been plotted (Fig. 5). Noteworthy is that the best mechanical contact is most difficult to reach in materials with higher porosity and larger particles.

Comparing the formation of electrical and mechanical contact shows that the quality of contact determined from electrical characteristics is better than that assessed from the elastic modulus. In view of the proposed method for determining the quality of contact, we conclude that mechanical contact forms somewhat later than electrical one in all cases. Electrical contact forms at a temperature about 50ºC lower than mechanical contact does (Fig. 6). It is seen that physical contact (K_e is calculated using Eqs. (12) and (13)) forms at higher temperatures than electrical and mechanical contacts do. Its formation also depends on the porosity and, to a lesser extent, on the powder fraction. This is due to the different mechanisms by which the contacts form.

DISCUSSION OF RESULTS

We will use Eq. (1) to calculate the capillary forces that act at interparticle boundaries of a titanium compact. The surface energy of titanium is known to be 1.24 J/m^2 at 20ºC [20]. A fracture analysis is used to assess the radius of curvature of the contact area from the size of the gap between powder particles. The size of interparticle gaps in a –0315+02 powder titanium compact varies from 0 to 3 μm (Fig. 7). Substituting the maximum size of the gap into Eq. (1), we obtain a capillary pressure of about 1 MPa.

There are ideas of what creep mechanisms are in titanium in the range of temperatures that correspond to our sintering conditions. Noteworthy are classical Frost–Ashby maps [21] plotted for titanium with grains 100 μm over a wide range of temperatures and strain rates. The creep mechanisms for low-alloy VT-1-0 titanium alloy in the temperature range of interest are detailed in [22]. Figure 8 shows relationship between the stress, temperature, and strain rate.

It is quite difficult to interpret strain rate in sintering. If we set 100% for complete filling of the contact area with atoms and 1 h for the duration of sintering, then the gap between particles fills for 1000 sec (~15 min) at a creep rate of $1 \cdot 10^{-3}$ sec^{-1} and for 10,000 sec (~3 h) at $1 \cdot 10^{-4}$ sec^{-1}. Hence, the contact will be 30% formed for 1 h at a creep rate of $1 \cdot 10^{-4}$ sec^{-1}. The experimental data show (Figs. 2 and 4) that this sintering rate is reached in titanium compacts at 700ºC.

Comparing this result with data from standard creep tests on titanium (Fig. 8), we may conclude that the creep rate in sintering is approximately one order of magnitude higher at the same stresses. This is because the papers [21, 22] analyze recrystallized titanium with grains 100 μm, while we study a material with deformed powder particles. According to [23], the deformation substructure substantially relieves the yield stress in deformed titanium above 600ºC. In particular, the stress decreased to one-third of its value at 700ºC and the creep rate may increase by one order of magnitude taking into account the sensitivity of the yield stress to the strain rate.

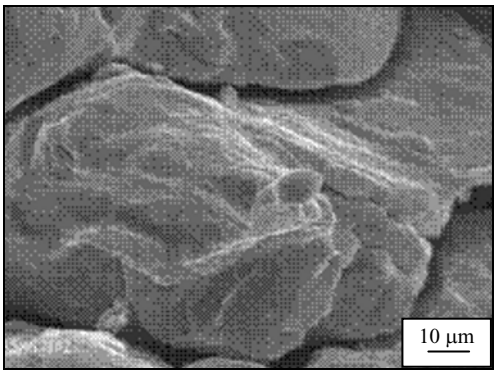

Fig. 7. Interparticle fracture surface of –0315+02 powder titanium compact

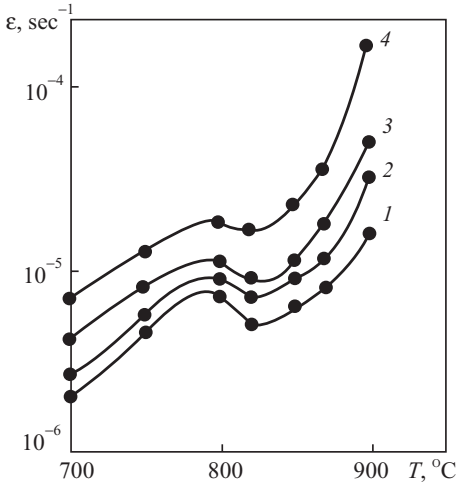

Fig. 8. Change in steady-state creep in $\alpha \rightarrow \beta$ transformation at stresses 0.5 (*1*), 0.9 (*2*), 1.2 (*3*), and 2.5 MPa (*4*) [22]

The effect of porosity on sintering is predictable: denser compacts are sintered faster (Fig. 5). However, note that the increase in conductivity and, thus, in the contact area for all porosities are practically commensurable at early stages of sintering (at 300ºC). The contacts existing in green state seem to start growing in all compacts at the same rate. Contacts in denser materials grow faster at sintering temperatures of 500 and 700ºC because of denser deformation-induced defects inside particles. Contacts in high-porous materials form much slower at later stages, which seems to be due to a great number of wide cracks and large pores that are healed at higher temperatures.

The particle size substantially influences the sintering temperature (Figs. 2b, 3, 4b, and 5). The size changes only due to contact formation since it is observed only at this stage. The mechanical and electrical properties are not sensitive to the particle size in green state [2] and after the formation of contacts. It seems that the size similarity condition [24] is met in pressed compacts, as is also the case for ideal spherical powders, according to which the size of pores and of contact radius is proportional to that of a particle. This assumption needs to be additionally studied, which is beyond the scope of this paper. Another possible reason of the faster sintering in compacts of smaller powder fractions is prevailing surface and grain-boundary diffusion within the contact area. The diffusion may be greatly influenced by the high density of dislocations in surface layers of particles in deformed compacts [2].

Therefore, the basic principles of sintering theory permit describing the structurization patterns in titanium-based powder materials. However, mass-transfer mechanisms in the sintering of titanium need to be examined in greater detail.

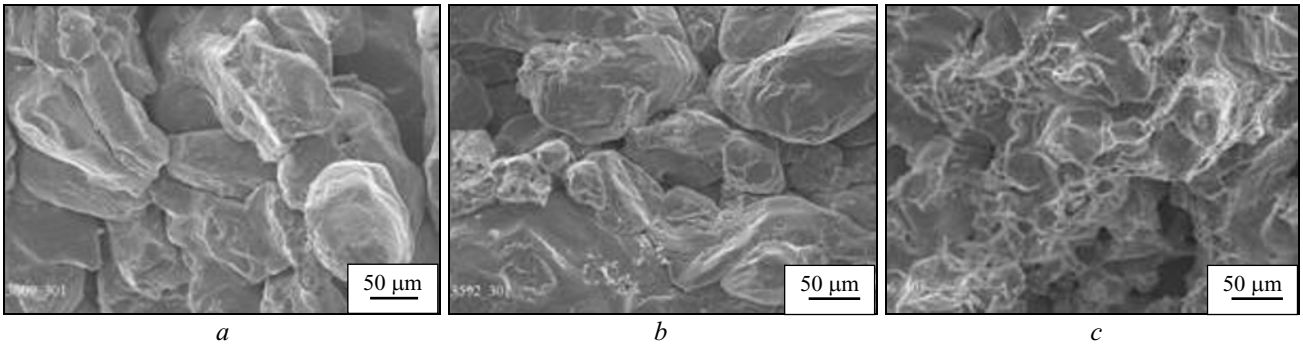

a *b* *c*

Fig. 9. Fracture pattern of 0315+02 titanium samples with 10% porosity sintered at 20 (*a*), 700 (*b*), and 1200°C (*c*)

Noteworthy is the substantial difference between K_λ and K_E determined on the same samples (Fig. 6). The experiments have shown that relative conductivity increases much faster than the elastic modulus does at the early stages of sintering. This seems to be determined by how a current flows through an actual contact [11]. In addition, it should be remembered that the contact area is treated differently when measured with electrical and mechanical methods.

Comparing the elastic moduli determined using standard mechanical tests and the dynamic method of mechanical resonance spectroscopy of a bar sample (Table 2) shows that the dynamic modulus is somewhat higher than the static one at the initial stages of sintering; but E and E_{dyn} become closer as the contact improves. The differences are due to change in the acoustic contact under a mechanical wave, in which tension and compression alternate. Particles that do not come into contact in free state and in the tension phase may come close in the compression phase due to elastic displacement, thus increasing the total contact area between them.

The physical contact forms at temperatures about 300°C higher than the mechanical one does (Fig. 6). The fracture analysis permits identifying what promotes and hinders the formation of the physical contact. The fracture patterns (Fig. 9) testify that the fracture of a sintered titanium sample continues by the interparticle mechanism at temperatures much higher than that at which the mechanical contact forms.

The low strength of the interface was discussed many times in cold welding theory [25, 26] and was attributed to the high concentration of admixtures near it. The strength of the interface may be increased by its recrystallization. A similar problem was solved in [16, 17] for powder iron. The abrupt increase in fracture toughness occurred when interparticle fracture changed to transcrystalline one and interparticle boundaries disappeared at these temperatures. The effect observed in titanium differs only in the changeover from interparticle to dimple fracture and in abrupt increase in the strain to failure, which was very low ($e = 0.3\%$), when the mechanical contact has formed. The high temperature at which the interface recrystallizes (1200°C) is due to its high thermodynamic stability associated with admixtures.

CONCLUSIONS

The basic ideas that the capillary forces play the determining role and creep is the major mass-transfer mechanism may completely apply to titanium compacts and may be used to describe the structurization in titanium-based powder materials.

The use of K_λ, K_E, and K_e to plot the quality of contact as a function of sintering temperature permits analyzing how the contact is formed at different temperatures and how the electrical, mechanical, and physical contacts are formed in compacts with the same structure.

It is shown that the contact forms between 500 and 800°C, which is revealed when the resistivity decreases (electrical contact) or the elastic modulus increases (mechanical contact). The electrical contact in titanium compacts forms at temperatures lower by 50 to 100°C than the mechanical one does, while the physical contact forms at much higher temperatures (1000–1100°C).

The formation of electrical and mechanical contacts naturally depends on porosity and initial particle size: $T_{50\rho}$ and T_{50E} increase with porosity and decrease with initial particle size.

Comparing the elastic moduli determined using standard mechanical tests and mechanical resonance spectroscopy of a bar sample shows that Young's dynamic modulus is somewhat higher than static one at the initial stages of sintering, but they become close as the contact improves. This may be because the acoustic contact area increases as the edges of pores that do not touch in free state close up in the compression phase during dynamic measurements.

REFERENCES

1. E. M. Borisovskaya, V. A. Nazarenko, Yu. N. Podrezov, et al., "Mechanical properties of powder titanium at different production stages. I. Densification curves for titanium powder billets," *Powder Metall. Met. Ceram.*, **47**, No. 7–8, 406–413 (2008).

2. E. M. Borisovskaya, V. A. Nazarenko, Yu. N. Podrezov, et al., "Mechanical properties of powder titanium at different production stages. II. Mechanical behavior of porous titanium compacts," *Powder Metall. Met. Ceram.*, **47**, No. 9–10, 538–545 (2008).
3. J. Frenkel, "Viscous flow of crystalline bodies under the action of surface tension," *J. Physics*, **9**, No. 5, 385–391 (1945).
4. B. Ya. Pines, "On sintering (in solid phase)," *Zh. Teor. Fiz.*, **16**, 737–746 (1946).
5. Ya. E. Geguzin, *Physics of Sintering* [in Russian], Nauka, Moscow (1967), p. 360.
6. V. V. Skorokhod, *Rheology-Based Theory of Sintering* [in Russian], Naukova Dumka, Kiev (1972).
7. V. V. Skorokhod and S. M. Solonin, *Physical and Metallurgical Fundamentals of Powder Sintering* [in Russian], Metallurgiya, Moscow (1984), p. 159.
8. O. I. Get'man, S. P. Rakitin, and V. V. Skorokhod, "Rheological and thermal activation analyses of the sintering kinetics of tungsten powders," *Powder Metall. Met. Ceram.*, **23**, No. 10, 764–768 (1984).
9. J. P. Jernot, J. L. Chermant, and M. Coster, "A new model to describe the variation of electrical conductivity in materials sintered in solid phase," *Phys. St. Sol. (A)*, **74**, No. 2, 467–475 (1982).
10. J. P. Jernot, M. Coster, and F. L. Chermant, "Model to describe the elastic modulus of sintered materials," *Phys. St. Sol. (A)*, **71**, No. 1, 141–147 (1982).
11. V. V. Skorokhod and I. M. Fedorchenko, "Conductivity of fine mixtures with imperfect contact between particles," *Dop. AN USSR*, No. 7, 756–759 (1959).
12. O. V. Roman, V. V. Skorokhod, and G. R. Fridman, *Ultrasonic and Resistometric Inspection in Powder Metallurgy* [in Russian], Vyshcha Shkola, Minsk (1989), p. 182.
13. R. Holm, *Electric Contacts Handbook*, Springer-Verlag, Berlin (1958).
14. A. V. Vdovichenko, Yu. N. Podrezov, and V. V. Skorokhod, "Mechanical resonance spectroscopy of interparticle boundaries in high-density iron powder compacts," *Powder Metall. Met. Ceram.*, **47**, No. 5–6, 366–372 (2008).
15. M. Yu. Bal'shin, *Science of Powder Metallurgy and Fiber Metallurgy* [in Russian], Metallurgiya, Moscow (1972), p. 335.
16. S. A. Firstov, Yu. N. Ivashchenko, Yu. N. Podrezov, et al., "Interparticle failure of iron powder materials," *Powder Metall. Met. Ceram.*, **30**, No. 4, 329–335 (1991).
17. S. A. Firstov, A. N. Demidik, I. I. Ivanova, et al., *Structure and Strength of Powder Materials* [in Russian], Naukova Dumka, Kiev (1993), p. 175.
18. G. T. Hahn and A. R. Rosenfield, "Local yielding and extension of a crack under plane stress," *Acta Met.*, **13**, No. 3, 5–35 (1965).
19. J. Gurland and N. M. Parikh, "Microstructural aspects of the fracture of two-phase alloys," in: *G. Liebowitz (ed.), Fracture—An Advanced Treatise*, Vol. 7, Academic Press, New York (1972), pp. 841–878.
20. G. V. Samsonov (ed.), *Properties of Elements, Part 1, Physical Properties* [in Russian], Metallurgiya, Moscow (1976), p. 600.
21. H. J. Frost and M. F. Ashby, *Deformation-Mechanism Maps*, Pergamon Press, Oxford (1982).
22. V. K. Pishchak, I. V. Moiseeva, and P. N. Okrainets, "High-temperature strength and physical properties of VT1-0 commercially pure titanium," *Metallofiz. Noveish. Tehnol.*, **23**, No. 9, 1243–1257 (2001).
23. V. F. Moiseev, A. Yu. Borodyanskaya, A. V. Kotko, and I. V. Moiseeva, "Dislocation structures and mechanical properties of α-titanium between 196 and 850°C," *Metallofiz. Noveish. Tehnol.*, **19**, No. 4, 50–59 (1997).
24. S. V. Belov, *Porous Materials in Mechanical Engineering* [in Russian], Mashinostroenie, Moscow (1981), p. 247.
25. É. S. Karakozov, *Solid-Phase Metal Bonding* [in Russian], Metallurgiya, Moscow (1976), p. 264.
26. Yu. L. Krasulin, *Solid-Phase Interaction of Metal with Semiconductor* [in Russian], Nauka, Moscow (1971), p. 119.